Why Do We Think We Have Found The Standard Model Higgs Boson?

NG Yui Ching Eugenius
of Imperial College London

A BSc Project (ASTRO) submitted to Imperial College London for the degree of Bachelors of Science in Physics.
Supervisor: Professor Gavin J. Davies
Assessor: Dr Per M Jonsson
Word Count: 5834

Abstract

The Standard Model Higgs boson was first theorised in 1964, leading to multiple experiments being conducted around the world, namely the LEP, Tevatron and the LHC, all with the goal of discovering this particle. Evidence for the Higgs was observed in LEP at 1.7σ and Tevatron at 3ÏČ confidence level. In the summer of 2012, the CMS and ATLAS collaborations independently discovered a new boson consistent with the SM Higgs boson with 5σconfidence at masses 125.3 ± 0.4 and 126.0 ± 0.4 GeV/c^2 respectively. In this paper, the data from these experiments will be analysed in an attempt to explain how the Higgs was discovered.

Declaration

This dissertation is the result of my own work, except where explicit reference is made to the work of others, and has not been submitted for another qualification to this or any other university. This dissertation does not exceed the word limit of 6000 words.

NG Yui Ching Eugenius

Acknowledgements

I would like to thank my supervisor Professor Gavin Davies, my assessor Dr Per M Jonsson

Contents

1 Introduction

The Standard Model is the physics model used by scientists around the world nowadays to decided what to expect in an experiment. It is taught in schools and Universities alike and is agreed to be the most up to date model on the Universe yet. It is, however, not without errors, and countless experiments were conducted to test its rigidness.

The SM Higgs boson is a particle that has fascinated and puzzled many. It was first realised to be a necessity in 1964, when a group of physicists, including the present day Nobel Laureates Peter Higgs and François Englert as well as Imperial professor Tom Kibble†, produced the 1964 PRL Symmetry Breaking Papers[1],[2],[3] to explain the phenomena described by electroweak symmetry breaking. Since then, it had proven itself to be one of the most mysterious and elusive particles to be discovered, with searches for it spanning over 4 decades. Until the Summer of 2012, it remains to be the only undiscovered particle that was predicted by the Standard Model.

2 Theory

In order to understand the problem proposed by electroweak symmetry breaking, the concept of a boson must first be revisited. A boson is a particle that enables different fermions to interact through its corresponding interaction. For example, a W boson allows a beta minus decay to happen through the Weak Force.

The 4 fundamental forces are the Electromagnetic Force, Weak and Strong Nuclear Force, and Gravity. Apart from Gravity, all of them are included in the Standard Model as well as having observed gauge bosons. Those are the photon for Electromagnetic Force, the gluon for the Strong Nuclear Force, and the W and Z bosons for the Weak Nuclear Force.

A problem arises with the gauge bosons: The SM predicts all of them to be massless[4], this is consistent with the massless photon and the gluon, but not with the W and Z bosons, which were observed to be massive.

This phenomenon can be explained by the Higgs mechanism, first proposed in 1963[4]. The idea was that the universe is penetrated by a scalar field known as the Higgs Field described by a non-zero minimum potential (Figure 1)[44]. Particles that interact with the field will take on a non-zero value and acquire a mass depending on the strength of that interaction, which can be seen more clearly on the Lagrangian[5] describing it. This is dubbed "spontaneous symmetry breaking" as the particle can spontaneously take any value on the minimum locus from the same initial conditions.

The Higgs Boson is believed to be the particle that enables fermions and certain other bosons to interact with the Higgs field. It is a scalar boson with a non-unity spin (unlike other gauge bosons) of 0+ as well as a neutral electrical charge as it corresponds to an electrically neutral polarisation component of the Higgs field[6].

2.1. Properties of the Higgs

Shortly after its theorisation 1964, not a lot was known about the Higgs Boson. An upper bound to its mass was set at $\frac{8\pi\sqrt{2}}{G_F}$ GeV/c2 ($\simeq$ 1000 GeV/c^2), where G_F is the

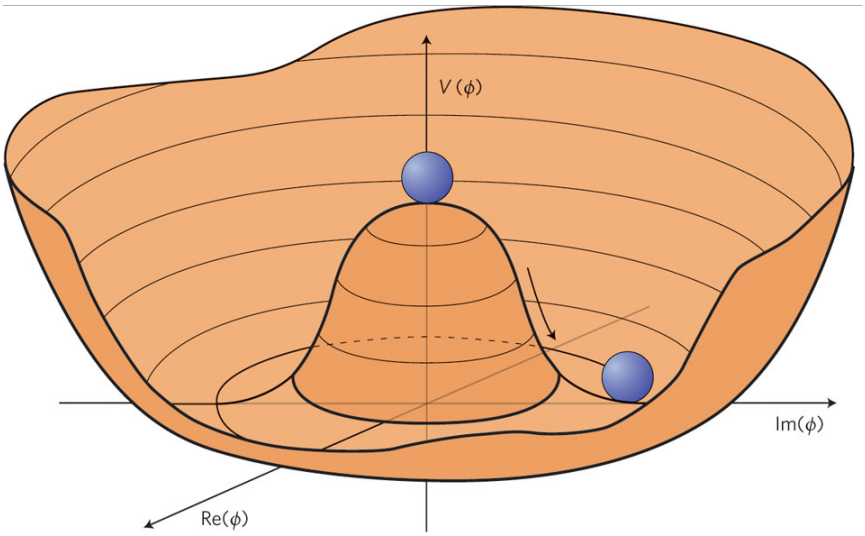

Figure 2.1.: Higgs Potential

Fermi Coupling Constant) using S-matrix-theoretic demonstration in 1977[7]. If the Higgs mass was to exceed this number, the weak force will turn into the strong force due to partial-wave unitarity not being respected by the tree diagrams for 2-body scattering of gauge bosons[7].

The lower bound for the Higgs Mass was deduced using a similar approach using different theoretical considerations. Using vacuum stability a lower bound of the Higgs was found to be $\simeq 4\ \mathrm{GeV/c^2}$, which was done in 1976[8].

The Higgs was also known to be a scalar boson due to the scalar nature of the Higgs Field, meaning that it has a non-unity spin, unlike all the other gauge bosons observed in the Standard Model. It also has an electrically neutral charge, as discussed in the theory section.

Knowledge of the Higgs' physical properties (such as spin and charge) and boundaries for its mass has allowed physicists to deduce some of its possible decay and production mechanisms. This was done[9] by estimating how it would interact through known physics along with applying known possible decay product masses to the proposed mechanisms, which enabled the existence of theoretical inconsistencies to be checked. This was an important process as it allowed a pathway to detect the Higgs through its decay products as well as an understanding of the methods to create it.

The possibilities of Higgs production from hadronic collision and as a result of decays of other particles were explored. For example, in a paper published in 1975[9], the production mechanisms

$$\pi^- p \longrightarrow H + n \tag{2.1}$$

$$\gamma p \longrightarrow H + p \tag{2.2}$$

$$pp \longrightarrow H + X \tag{2.3}$$

$$\eta \longrightarrow \pi^0 + H \tag{2.4}$$

$$\Sigma^0 \longrightarrow \Lambda + H \tag{2.5}$$

$$K^+ \longrightarrow \pi^+ + H \tag{2.6}$$

$$e^+ e^- \longrightarrow Z^0 + H \tag{2.7}$$

as well as the decay modes

$$H \longrightarrow e^+ e^- \tag{2.8}$$

$$H \longrightarrow \mu^+ \mu^- \tag{2.9}$$

$$H \longrightarrow \pi^+ \pi^- \tag{2.10}$$

$$H \longrightarrow \gamma\gamma \tag{2.11}$$

were investigated in detail for various energies. Analysis of their individual differential cross sections and decay widths along with the ratio of those values to the corresponding alternative reaction (eq. 3.1 and the reaction $\pi^- p \longrightarrow \rho^0 + n$) led to the realisation that most of those reactions have a small probability of occuring (107 to 108 times more infrequent than the alternate reaction)[9]. The paper proved to be inconclusive for if the Higgs boson mass exceeds 5 GeV/c^2 , and ended with a discouraging note on any large scale experimental search for the Higgs.

2.2. How can the Higgs be discovered?

Not discouraged by the unpromising atmosphere, physicists have begun testing for the Higgs in as early as 1989 in the Large Electron and Positron Collider (LEP) at CERN, later expanding into Tevatron in the Fermi National Accelerator Laboratory (Fermilab) in USA, and finally in the Large Hadron Collider (LHC) back at CERN, where the 2012 discovery took place.

As it turned out, the production modes that proved to be the most useful in those colliders were production via (eq. 2.3, 2.7), along with gluon fusion (production through gluon fusion into a top quark loop, abbreviated ggH), vector boson fusion (production from fusion between 2 quark originating W/Z bosons, abbreviated VBF), Higgs Strahlung (production through radiation from a W/Z boson) and top quark fusion (production through 2 gluon originating top quarks, abbreviated ttH)[5]. The Feynman diagrams for the dominant ggH and Higgs Strahlung production modes are shown in figure 2.2[5].

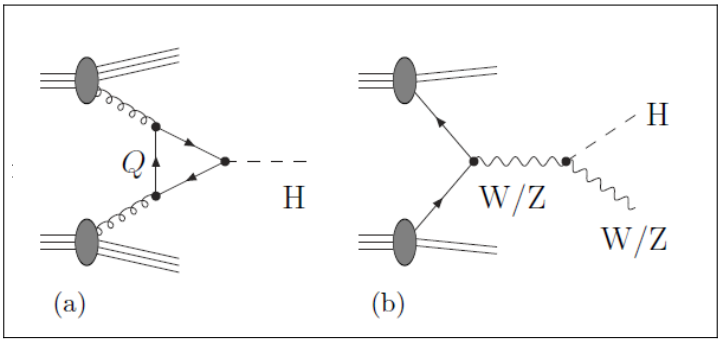

Figure 2.2.: Feynman diagrams of a) ggH and b) Higgs Strahlung production

The main decay modes used to analyse Higgs activity were through (eq. 2.9), (eq.2.11) along with decay into a bottom quark and its antiparticle counterpart, 2 W/Z bosons and their respective antiparticle, 2 taus, 2 gluons, a charm quark and its and its antiparticle, and finally a Z boson and a photon. Shown below are the equations for those reactions as well as the Feynman diagrams (Figure 2.3)[5] for the diphoton and the ZZ decay mode.

$$H \longrightarrow b\bar{b} \tag{2.12}$$

$$H \longrightarrow WW^* \longrightarrow 4l \tag{2.13}$$

$$H \longrightarrow ZZ^* \longrightarrow 4l \tag{2.14}$$

$$H \longrightarrow \tau^+\tau^- \tag{2.15}$$

$$H \longrightarrow gg \tag{2.16}$$

$$H \longrightarrow c\bar{c} \tag{2.17}$$

$$H \longrightarrow Z\gamma \tag{2.18}$$

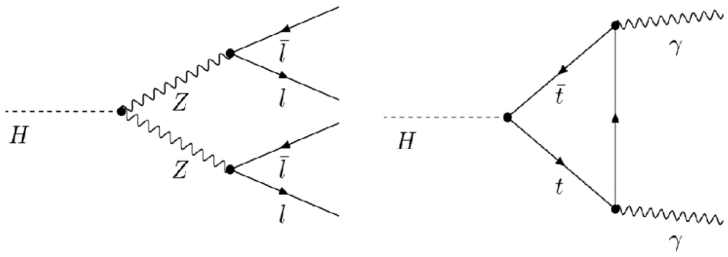

Figure 2.3.: ZZ decay mode and (left) and diphoton decay mode (right)

Events were simulated using Monte Carlo (MC) event generation method in conjunction with next-to-leading order (NLO) matrix elements[10]. For reference, the simulated branching ratios for different Higgs mass ranges from 90 GeV to 1000 GeV is included in the appendix[11]. At low energies (<100 GeV) the dominant decay mode was (eq. 2.12), taking up more than 90%, followed by (eq. 2.10). Decay through (eq. 2.11) was very infrequent, with a branching ratio of less than 0.1%.

As the energy increased from 100 GeV to 200 GeV the dominant b quark decay mode began to drastically decrease and the vector boson decay modes described by (eq. 2.13) and (eq. 2.14) gradually rose to be the dominant ones. This trend remained all the way up to the 1000 GeV boundary.

Using simulated data, the expected number of decays and hence the expected signal strength at a given energy for the different decay modes could be computed. This in turn could be used to be compared to a background signal to measure the significance of the signal as compared to the background.

Imagine the background signal at any energy to be modelled by a normal distribution, with the mean (also the mode) of the distribution centered at 0. The fluctuations of that signal can in turn be converted into a numerical standard deviation value.

Using those 2 properties, the situation can be viewed statistically as a hypothesis test with the null hypothesis set as the background hypothesis (no Higgs exist, the background is the only contribution to the signal detected in the detectors). The 68-95-99 rule can be applied to the background hypothesis as it is a gaussian distribution (Figure 2.4).

Typical hypothesis testing will set the significant level at 5% – or 2σ (standard deviation) level confidence. Here the p-value (probability of observing data beyond the selected significance level given the null hypothesis) is 0.05. In the cases of scientific discoveries, 2σ is not good enough, as the p value is still relatively high - occurring once in every 20 measurements.

It is more customary to start documenting measurements that occur over 3σ from the mean. This has a p-value of 1.5×10^{-3} - occurring once in every 667 measurements. This is more improbable than a 3σ measurement, but not improbable enough to term a scientific discovery (considering the massive amount of data collected at the particle colliders). Instead data observed at a 3σ confidence are termed "evidence for". This was the confidence level observed at Tevatron.

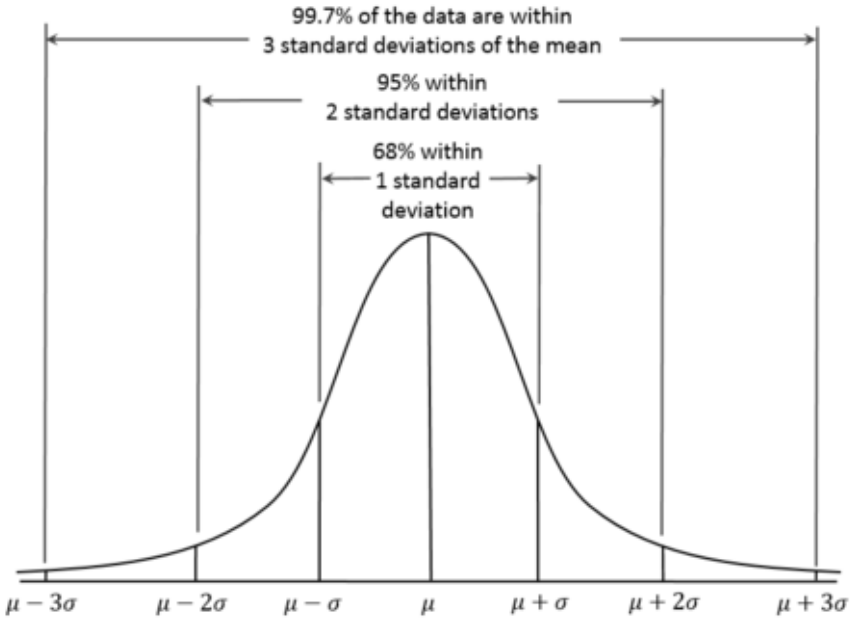

Figure 2.4.: The 68-95-99 rule describing the percentage of data that lies within 1, 2 and 3ÏČ (standard deviation) of the mean[45]

For data to be considered sufficient enough to term as a scientific discovery, the measurement must occur above 5σ from the mean[12]. The corresponding p-value for this confidence level is 3×10^{-7}, meaning a frequency of once every 3.3 million measurements - a significant decrease in likelihood in the order of 10^{-4}. This was the significance level observed by the CMS and ATLAS collaboration in the 2012 discovery.

3 Seraches before the discovery

3.1. Large Electron-Positron Collider (LEP)

As mentioned in section 2.2, searches for the Higgs has commenced since the 1980s. One of the first particle colliders to test for the Higgs was the LEP in CERN. Construction for LEP started in 1983 and took 6 years to complete. Multiple infrastructures were built, including the well known 27km ring that housed the accelerator, which finished in 1988[13].

Up until its closure in 2000, LEP had been searching for the Higgs using its 4 detectors: ALEPH, DELPHI, L3 and OPAL. The entire collider housed 5176 magnets and 128 accelerating cavities[13]. For the initial 7 years of its running the collider operated at a centre of mass (CoM) energy of up to 100 GeV/c2 [13]. In 1995 LEP was upgraded, with 288 superconducting accelerating cavities added to double the operating energy[13].

Before its final year of running LEP data provided no indication of the production of a Standard Model Higgs boson. This prompted LEP to raise the CoM energy of the positron-electron collision up to 209 GeV in its final year of running[13].

LEP mainly used the mechanism outline by (eq. 2.7) for Higgs production[14] aided by a small contribution from the Higgs Strahlung process as well as the VBF process. For the energy range that LEP investigated, the major decay mode is the one described by (eq. 2.12), taking up 74% of the branching ratio, followed by (eq.2.13, 2.15, 2.16) with each occupying 7% of the branching ratio. The remaining 4% is constituted by (eq. 2.17).

MC simulation method was used in all 4 collaborations to simulated expected signal and background measures for different hypothetical Higgs masses. This took into account any non-Gaussian contributions the experimental conditions might have, such as the centre of mass energy as well as the integrated luminosities (amount of particles passing a given point at given time) of the data samples[14].

The binned likelihood of the signal+background (S+B) hypothesis (Higgs contributes to the data set) was compared to that of the background (B) hypothesis (Higgs doesn't not contribute to the data set). Using observed data, separate χ^2 tests were conducted on the B and the S+B hypotheses. The difference between the 2 different χ^2 tests was calculated, this is done by computing the test statistic given by

$$-2ln\left(\frac{\mathcal{L}_{S+B}}{\mathcal{L}_B}\right) \tag{3.1}$$

The fraction in the parenthesis represent the ratio between the binned likelihood of the S+B and B hypothesis, it is sometimes expressed as Q. The combined results from all 4 collaborations are shown in Figure 3.1[14].

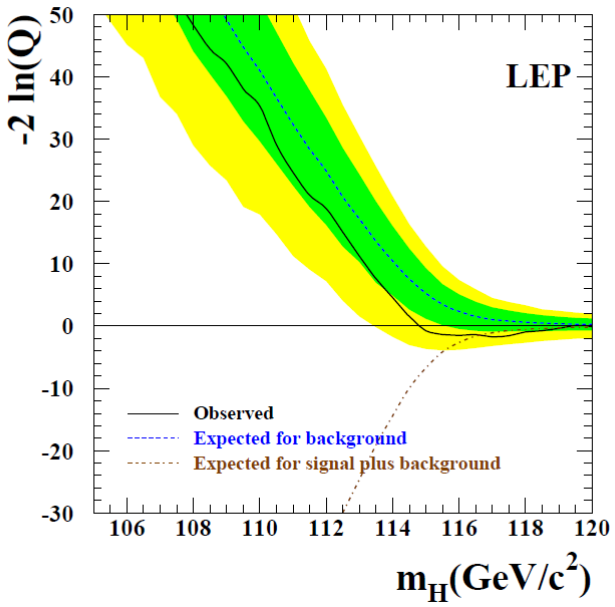

Figure 3.1.: Observed difference in χ^2 test between the 2 hypotheses in the range $105 < M_H < 120$ GeV/c^2

From the graph it can be seen that the S+B hypothesis started to become viable at around the hypothetical Higgs mass (M_H) of 115 GeV/c^2, with the negative value of the test statistic suggesting the B hypothesis being disfavoured in energies greater than 115 GeV/c^2.

A clearer analysis of the test statistic involves analysing its expected spread for different specific Higgs mass for both hypotheses. Comparing this to the observed test statistic visualises its compatibility with both hypotheses. This can be seen in

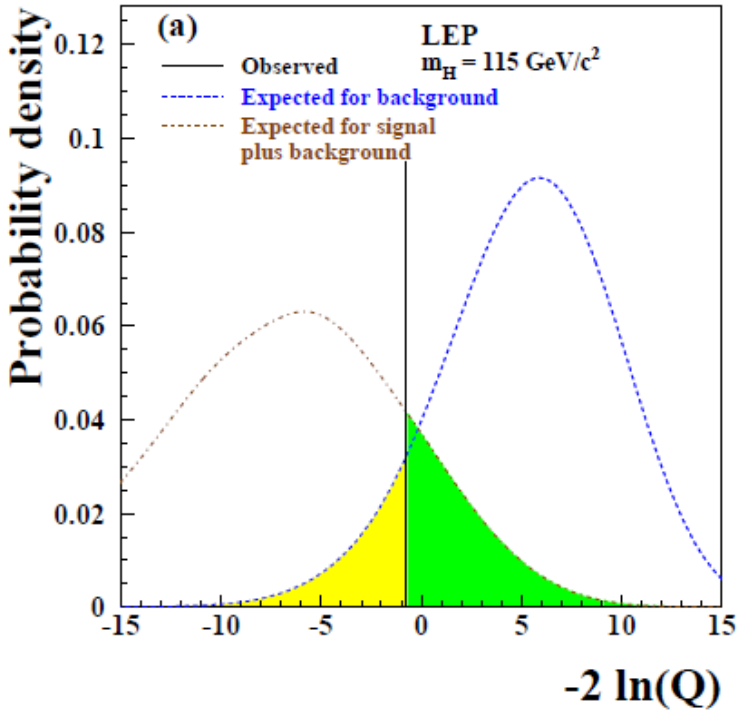

Figure 3.2.: The PDF distribution of the test statistic for the S+B hypothesis as well as the background hypothesis at $M_H = 115$ GeV/c^2. The yellow region represents $1 - CL_b$ and the green region represents CL_{s+b}

	$1 - \mathrm{CL_b}$	$\mathrm{CL_{s+b}}$
LEP	0.09	0.15
ALEPH	3.3×10^{-3}	0.87
DELPHI	0.79	0.03
L3	0.33	0.30
OPAL	0.50	0.14
Four-jet	0.05	0.44
All but four-jet	0.37	0.10

Table 1: $1 - CL$ and CL_{s+b} values for all 4 collaborations and their combined values

Figure 3.2 for the case where M_H=115 GeV/c^2. 2 other such plots for M_H=110 and 120 GeV/c^2 can be found in the appendix (Figure 23)[14].

A trend could be seen from those 3 plots in that the distributions between both hypotheses overlap more as M_H increases, the increased overlap of those 2 distributions decrease the ease of discrimination of the compatibility of the observed test statistic with the B and the S+B hypotheses.

Regarding those values, the former of was calculated by integrating the B hypothesis PDF from $+\infty$ to the observed value, it is notated by $1 - CL_b$, and is equivalent to the p-value as discussed in section 2.2. The latter was calculated by integrating the S+B hypothesis PDF from $-\infty$ to the observed value and is notated CL_{s+b} and can be interpreted as the p-value for the S+B hypothesis[14]. Those values are easily visualised on Figure 3.2, and were calculated for the 4 different collaborations. Table 1[14] shows those values for $M_H = 115$ GeV/c^2.

The overall result from LEP provided no straightforward conclusion regarding the compatibility of the observed test statistic and both hypotheses. The background p value of 0.09 shown in Table 1 only corresponded to a standard deviation confidence of 1.7σ (see figure (number) in appendix) – nowhere near the 3σ needed to term as "evidence for" the Higgs boson.

A lower bound for the Higgs was however derived using the ratio

$$CL_s = \frac{CL_{s+b}}{CL_b} \tag{3.2}$$

This quantity was calculated for MH in the range 100 to 120 GeV/c^2, shown in Figure 3.4[14].

As can be seen the observed CL_s crosses the $CL_s = 0.05$ line at $M_H = 114.4$ GeV/c^2. This set a lower bound for the Higgs mass of 114.4 GeV/c^2 at a 2σ (95%) level, as the value for CL_s was too small below this mass for the consideration of the S+B hypothesis.

Those were the data taken from the LEP1 and the LEP2 runs. The significance level was, although too small for a discovery to be termed, sufficient enough to point at a specific mass region for LEPâĂŹs successor LHC to work on.

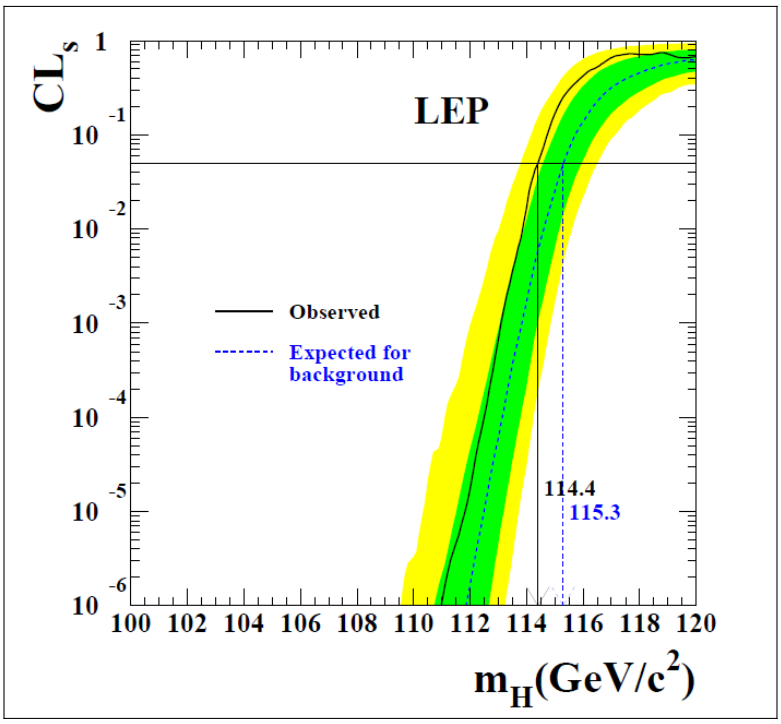

Figure 3.4.: Relationship between CL_s and MH in the range $100 < M_H < 120$ GeV/c^2

3.2. Tevatron

Tevatron was completed in March 1983 and started running in July of the same year. Buried 7.6 metres underground, it was the largest particle collider in the US, and the second largest particle collider in the world with a circumference of 6.4km[15].

Making use of its 2 detectors D0 and CDF, data was collected and analysed from proton antiproton collisions through its accelerator ring initially known as the Energy Double/Saver. Initial runs accelerated protons at a CoM energy of 512 GeV and quickly rose to 800 GeV in 1984[16], the accelerator ring was renamed to Tevatron after it managed to accelerate protons to an energy of more than 1 TeV[16].

Tevatron would continue to run for more than 20 years, making cutting-edge discoveries in Run I and II (starting 1983 and 2001 respectively), those include the top quark (1995)[16], the B_c meson (1998)[16] and the Ω_{b^-} baryon (2008)[16] in the process, until its eventual shut-down in 2011.

The main Higgs production channels that used were VBF, ggH and associated production with a vector boson, those were achieved by colliding proton and antiproton

beams at a CoM energy of 1.96 TeV. The decay modes outlined by (eq. 2.11, 2.12, 2.13 and 2.15) were utilised to measure Higgs activity[17], [18].

As with LEP, the expected signals were determined using the computer simulation. For CDF, the background signals were simulated using MC in conjunction with packages including Pythia[19] and ALPGEN[20]. D0 used a similar approach, using MC in conjunction with the mentioned packages as well as SINGLETOP[21] to simulate background signals[18].

The expected Higgs boson signal were computed using leading order (LO) calculation from Pythiawith CDF using the CTEQ5L parton distribution function (PDF) and D0 using the CTEQ6L1 PDF[22]. The ggH and VBF production processes were being simulated using NNLO (next-to-next-to-leading-order) in QCD (quantum chromodynamics), whereas the ttH production process was simulated using the MSTW 2008 PDF[23], [18].

The log likelihood (LLR) distribution of the 2 distributions along with their ratio was calculated in the range $M_H = 90$ to 200 GeV/c^2. The result is shown in Figure 3.5[18].

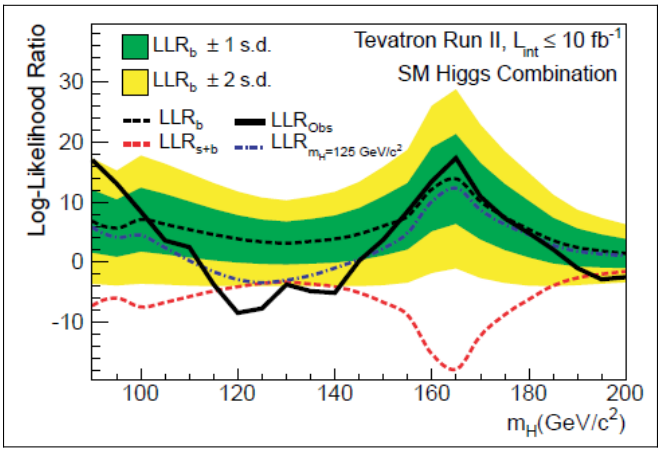

Figure 3.5.: Observed LLR for along with its expectation value under the B and S+B hypothesis. Shown also is its expected value under a S+B hypothesis of $M_H = 125$ GeV/c^2

A detailed table of those values can be found in the appendix. The observed LLR is $> 2\sigma$ away from the background expectation at around $M_H = 120$ GeV/c^2, and consistent with the simulated LLR signal assuming the existence of a SM Higgs boson with a mass of 125 GeV/c^2. As can be seen, it also reverts to background-like at around $M_H = 150$ GeV/c^2, discouraging hypothetical Higgs masses around that mass region.

A clearer comparison was made by including the 2σ limit of the expected signal under the B hypothesis with the observed ones. The result is shown in figure 3.6[18].

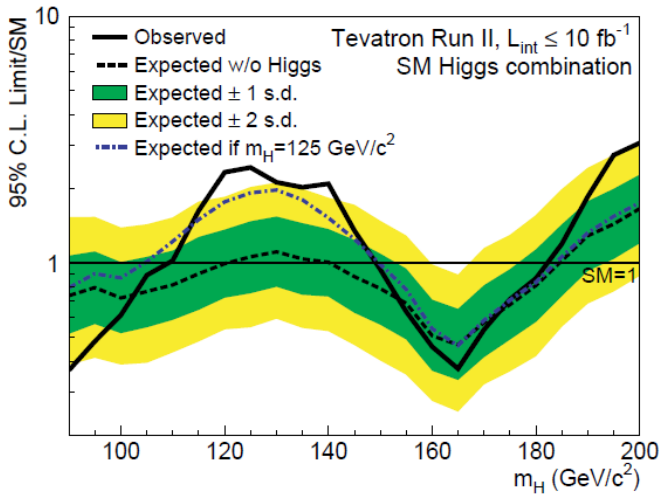

Figure 3.6.: Expected signal events with their 1 and 2σ fluctuations for the B hypothesis along with the observed values. Included is also the expected signal assuming the existence of a Higgs boson at a mass of 125 GeV/c^2.

The inclusion and exclusion range can be inferred directly from the graph. The Higgs mass should be excluded for all mass ranges where the observed signal is below 2σ to the SM background expectation, as it is safe to assume the absence of the Higgs if the signal doesnâĂŹt exceed even 2σ from the background expectation value.

Conversely, the Higgs mass should be included in mass ranges where the observed signal is $\geq 2\sigma$ from the background using the same logic. From the graph it can be seen that the Higgs mass can be included within 109 GeV/c^2 $< M_H <$ 149 GeV/c^2[17] at a 95% confidence, with the exclusion regions being 90 GeV/c^2 $< M_H <$ 109 GeV/c^2[17] and 149 GeV/c^2 $< M_H <$ 182 GeV/c^2[17].

The observed signals and their corresponding background p-value were calculated and plotted in the same mass range, this is shown in Figure 3.7[18]. The background p-value for the observed signal can be seen to dip to over 3σ from the B hypothesis at around $M_H = 120$ GeV/c^2, disfavouring the B hypothesis. The observed signal can also be seen to be compatible with the S+B hypothesis, as can be seen by its similarity with the curve line representing the expected background p-value with the assumption of the existence of a Higgs boson at $M_H = 125$ GeV/c^2.

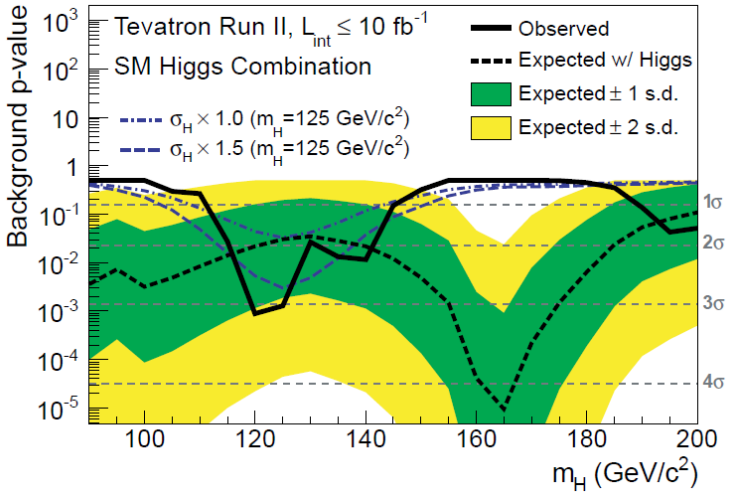

Figure 3.7.: Observed and expected p-values of for the B and S+B hypothesis

From the above data, an inclusion range for the Higgs mass can be set between 109 GeV/c^2 and 149 GeV/c^2 at a 95% confidence level, as well as the observation of the evidence for a SM Higgs boson at MH between 120 GeV/c^2 and 125 GeV/c^2 at a 3σ level confidence. This concludes the data taken from Tevatron[17],[18].

4 LHC and the discovery of the Higgs

4.1. Detector Concepts

Utilising the 27km collider rings that LEP had, the LHC started running in September 2008 with the aim to discover the Higgs boson and measure its properties as well as tests for dark matter and the manner in which matter evolved from the early Universe[24].

The 4 different particle detectors, namely CMS, ATLAS, ALICE and LHCb, were positioned around the accelerator ring to collect and analyse data taken from proton proton collisions with a CoM energy of up to 8 TeV[24]. Of which the CMS and ATLAS detectors would succeed in independently discovering a particle consistent with the SM Higgs boson.

The CMS, shorthand for Compact Muon Solenoid, is a detector made from a giant solenoid magnet. A steel yoke confines the giant magnetic field created by the solenoid, and is responsible for its heavy weight of 1.4×10^6 kg[24]. The CMS

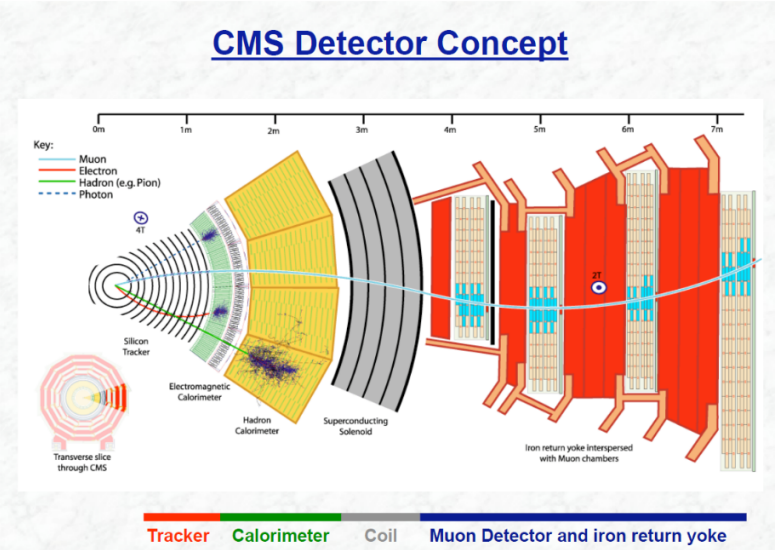

Figure 4.1.: The CMS detector concept[24]

(shown in Figure 3.7) is consisted of 4 main regions: The tracker, the electromagnetic calorimeter (ECAL), the hadronic calorimeter (HCAL) and the muon spectrometer.

The tracker is mainly made up of silicon - a light material to minimise the disruption to the final tracking output. It is made up of 65 million pixels and spans a total silicon surface area of 198 m^2[25]. In terms of path reconstruction it is able to accurately (up to $10\mu m$[25]) reconstruct paths for all types of hadrons as well as the muon and the electron by plotting their trajectory when they pass through the magnetic field generated by the solenoid. It tracks particles within the range

$$|\eta| < 2.5 \tag{4.1}$$

Where the quantity η can be expressed as

$$\eta = -\ln[\tan\left(\frac{\theta}{2}\right)] \tag{4.2}$$

With θ being the polar angle measured from the positive z axis (anticlockwise beam direction)[25].

The ECAL is made up of around 80,000 $PbWO_4$ crystals, it is dedicated to measuring photons and electrons (abbreviated e/γ) with a high intrinsic resolution[26]. When high energy electrons or photons collide with the crystals, they excite the electrons in those crystals to a higher orbit. Those crystals will reveal the presence of electrons and photons by emitting bursts of photon in proportion to the energy lost (and hence the penetrating particle) when the exited electron returns to the ground state, this process is called scintillation. The photons are then converted into amplified electrical signals that are sent off for analysis[26].

The HCAL is made up of over a million WW2 brass shell casements taken from the Russian Navy. Designed to detect hadronic particles, it does so by taking advantage of a "showering" process caused by the collision of hadronic particles with the brass absorber plates. In this process, the portion of the absorber that experiences contact with hadronic particles emits secondary particles and starts off a chain reaction[27].

The resulting particles would eventually be absorbed by scintillation materials that emit light to be analysed, similar to the process in ECAL[27].

The final part of the detector is made to detect muons (created from the end products of (eq. 2.13)) that penetrate the rest of the experimental setup. This is done by exerting a strong magnetic field onto the muons and measuring the deflection in their path in conjunction with tracking their position through multiple layers of muon stations[28], which enables a value for their momentum to be calculated.

The 7×10^6 kg ATLAS detector is made up of the same 4 main components as the CMS and operates through the same principles. Some minor differences arise in their structural configuration, material composure and physical properties.

ATLAS utilises liquid argon and lead absorbers as the ECAL components to maximise the granularity of the observed data and also increase the stability of the ECAL itself by making it more radation resisant[29]. In addition, ATLAS produces a magnetic field half as strong as that of CMS[30], which causes a significant difference in the deflection of charged particles between the 2 detectors. Finally, the CMS places its ECAL and parts of its HCAL inside the solenoid to maximise the e/γ resolutions, which ATLAS has chosen not to do.

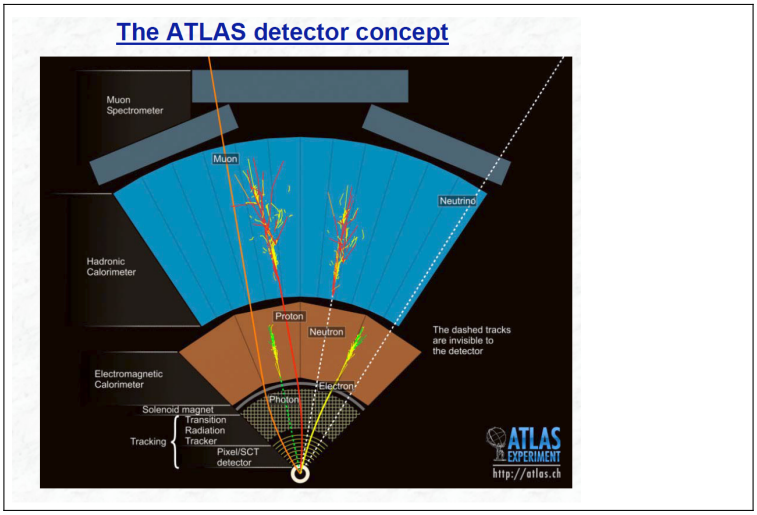

Figure 4.2.: The ATLAS Detector[30]

4.2. CMS Diphoton and ZZ decay data

As with the Tevatron, Higgs events were simulated through MC method using the Pythia 6.4-interfaced POWHEG[31],[32], which generates next-to-leading-order (NLO) matrix elements. The dominant ggH production process was replicated using the next-to-next-to-leading-logarithmic (NNLL) +NLO using the HqT package[33].

4.2.1. CMS Data

The CMS detector measured Higgs activity from proton-proton collisions with a CoM energy of 7 and 8 TeV through utilising the decay modes (eq. 2.11, 2.12), 2.13, 2.14 and 2.15)[5],[34],[35]. Of those, (eq. 2.12, 2.13 and 2.15) have low mass resolution due to the production of neutrinos from the final products of (eq. 2.13) and high background contributions that afflict measurements based on (eq. 2.12 and 2.15). The highest contributing modes are (eq. 2.11 and 2.14) due to their high mass resolution caused by the lack of by products in their final state.

The diphoton decay mode (eq. 2.11) had a large irreducible background from the QCD production of 2 photons as well as a reducible background from the misidentification of collision jet fragments, which occurs duing the Higgs mass reconstruction. For the detecton of the diphoton decay mode itself, a boosted decisition tree (BDT)[36] was used to output data that correspond to diphoton decay signals based on the quality of the observed signal as well as how its properties such as mass resolution and spread compares to that of the expected signal[34].

Events are reconstructed based on the CMS "particle flow" algorithm[37],[38] with data combined from the detectors. This process includes identifying particles' identity, which is important as it allows their momentum to be determined. Figure 4.3[34] shows the combined observed p-value along with the expected ones.

A more iconic graph shows the weighted events of the diphoton decay mode from 100 to 160 GeV/c^2 along with the background expectation value, shown in Figure 4.4[34].

Both graphs showed an inconsistency of the observed signal compared to the B hypothesis. Figure 4.4 showed an excess of events observed at around $M_H = 125$

GeV/c^2 while Figure 4.3 shows the observed p-value to be an order of 10-3 smaller than the expected one.

The ZZ decay mode (eq. 2.14) was searched through the 4 lepton state that it eventually ended up in, which could be $4e$, 4μ and $2e2\mu$. It had an irreducible background contribution stemming from direct ZZ mesons productions from $q\bar{q}$ and gluon gluon processes[34]. Reducible contributions vary for different lepton states, the most common ones are from $Z + b\bar{b}$ and $t\bar{t}$ productions[34].

Event selections for this decay mode are based on the properties of the observed 4 lepton states. They need to be 2 pairs of leptons that have the same flavour with opposite charge, with 1 pair's required invariant mass to be between 40-120 GeV and the the other 12-120 GeV. Expected event rates in the interested region (the signal region) is done by extrapolation from those calculated for the background control region[5],[35].

As with the diphoton decay mode, an excess of events was observed at around $M_H = 125$ GeV/c^2 which is consistent with the expected signal for a Higgs boson of mass 125 GeV/c^2. This is shown in Figure 4.5[34].

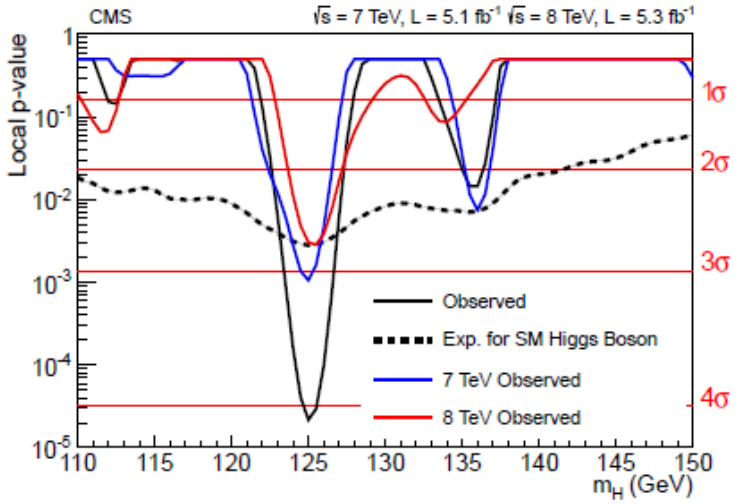

Figure 4.3.: The expected and combined observed local p-values from 7 and 8 TeV data sets for the diphoton decay mode

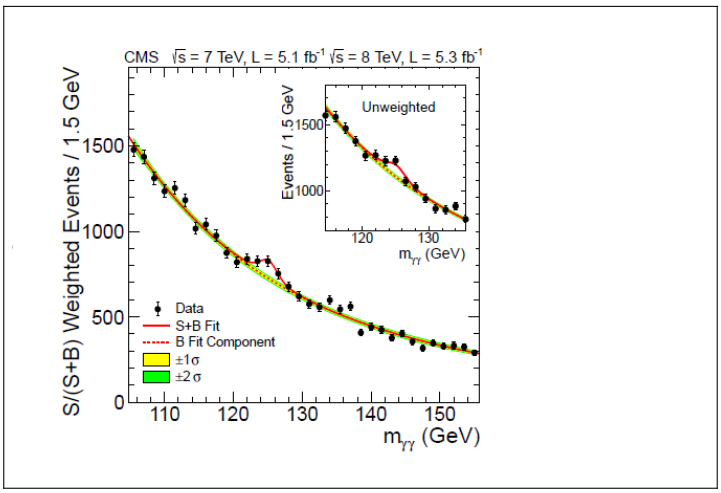

Figure 4.4.: Weight events of diphoton decay

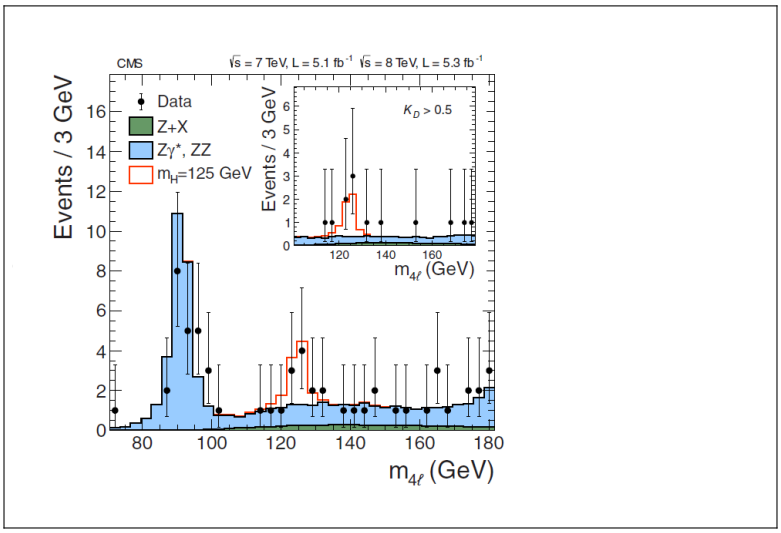

Figure 4.5.: Distribution of 4 lepton invariant mass compared to background expectation.

4.2.2. ATLAS data

ATLAS utilised the same algorithms and packages that CMS did to simulated Higgs production and decay modes. The exact expected branching ratios were calculated using the HDECAY[39] and PROPHECY4F[40] programs[41].

Using the same pp collision beams that the CMS did, the ATLAS collaboration measured Higgs activity through identical decay channels. The diphoton and ZZ decay modes were again valued over others due to their high mass resolution, with the same background contributions applying here as they did in the CMS[5],[41].

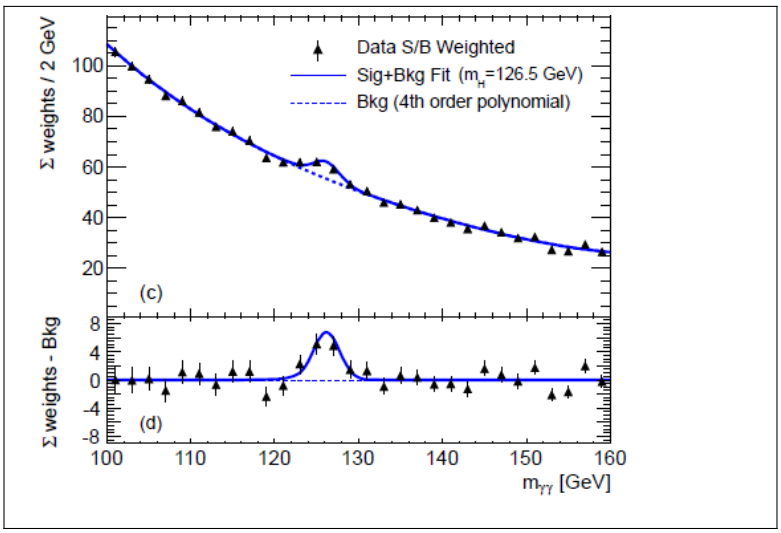

Figure 4.6.: Observed diphoton weighted events (top) and residual values (bottom) between 100 and 160 GeV

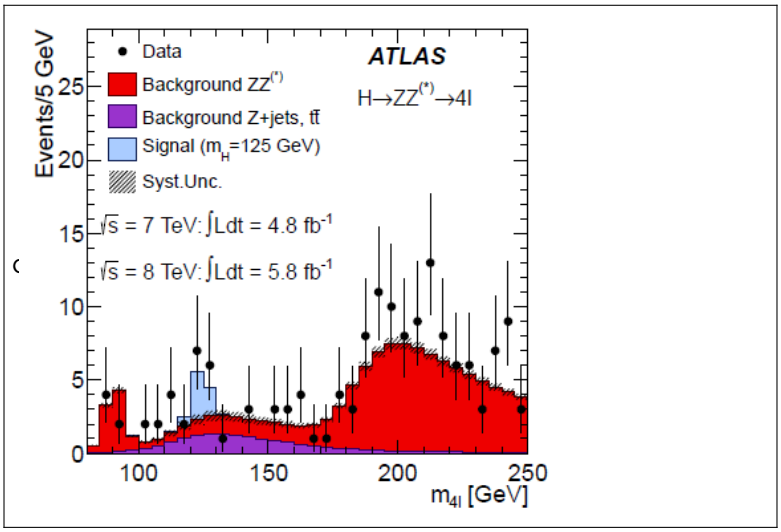

Figure 4.7.: Weighted events of 4 lepton decay mode between 90 and 250 GeV

An analytical method akin to that of Figure 4.4 was made. The observed diphoton weighted events in the range 100-160 GeV/c^2 can be found in Figure 4.6[41] with the background signal being modelled by a 4^{th} order Bernstein polynomial[34].

A similar analysis was performed on the 4 lepton decay mode, investigating the observed distribution of the 4-lepton invariant mass with that of the B hypothesis, as shown in Figure 4.7[41]:

Both decay mode's event distribution graphs displayed an excess of events at around $M_H = 125$ GeV/c^2, which agreed with their counterpart provided by the

CMS collaboration. This was promising as all the data agreed to a signal-like excess of events at the same mass region which lies within the mass limits set by LEP and Tevatron.

4.3. Combined data from CMS and ATLAS

A better conclusion can be made using data taken from all the decay modes. By individually analysing their respective agreement to the B hypothesis and taking into account their measurement reliability, the combined observed and expected event excess was calculated and compared to determine the overall compatibility of the data provided by CMS and ATLAS with the B and S+B hypothesis.

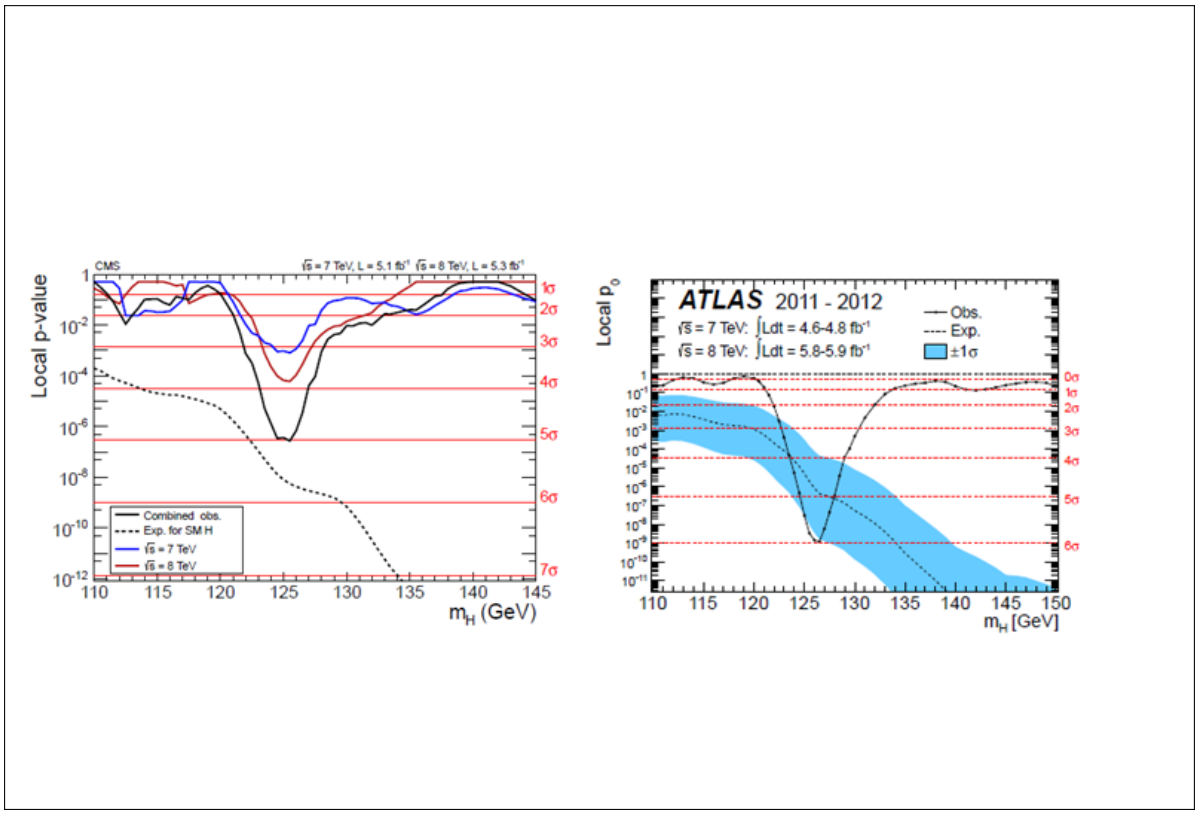

Figure 4.8.: Combined observed p-value from all the decay modes taken from the CMS collaboration (left) and ATLAS collaboration (right)

Displayed in Figure 4.8[34],[41] is the observed local p-value using all combined data from the CMS experiment and ATLAS. For CMS an overall event excess is observed at up to 5σ at $M_H = 125 \pm 0.4$ GeV/c^2[34] under the B hypothesis and consistent with the expected significance of 5.8σ. ATLAS also agreed with its respective

combined data with a combined observed local p-value at 6.0σ under the B hypothesis compared to the expected 5.0σ at $M_H = 125 \pm 0.4\ \mathrm{GeV/c^2}$[41].

4.4. Did it agree with the SM predictions?

An important aspect to address is the consistency of the properties of the observed particle with that which would be expected from SM predictions. This includes the compatibility of the observed mass (discussed above), spin-parity and couplings to different particles.

To measure the consistency of the Higgs coupling to different particles a signal strength modifier given by

$$\mu = \frac{\sigma}{\sigma_{SM}} \tag{4.3}$$

was defined. Here σ is the observed Higgs production cross sections multiplied by the relevant branching ratios, and σ_{SM} their respective expected value under SM simulated predictions. If the observed boson is indeed the SM Higgs boson, μ would take on the value of unity[35]. A detailed account of μ observed in the CMS and ATLAS for different decay modes is shown in Figure 4.9[5].

The individual decay modes are also separated into their different production taggings. Most of the measurements taken from both collaborations are compatible with unity, which shows the consistency of the CMS and ATLAS-observed boson to the SM Higgs predictions.

Further analysis was made on the coupling consistency by defining a kappa parameter

$$\kappa = \sqrt{\mu} \tag{4.4}$$

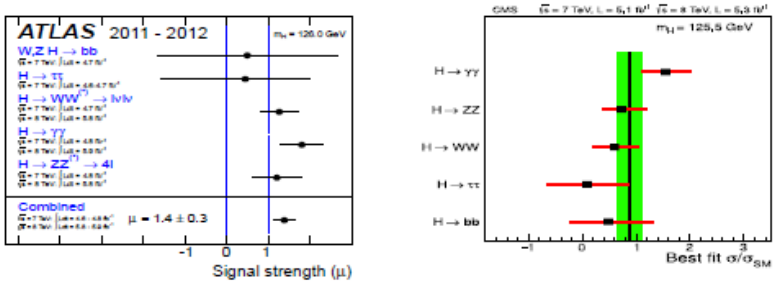

Figure 4.9.: Observed Higgs coupling compared to expected values for CMS (left) and ATLAS (right)

Where Îž could represent the coupling of the Higgs to vector bosons (κ_V), fermions (κ_f), gluons (κ_g) and photons (κ_γ). As with the case with Îij, all the different Îž need to take on a value of unity for consistency with SM predictions[35].

Likelihood scans were performed for different Îž values from different decay modes. An example can be seen in Figure 4.10[35].

The point (κ_γ,κ_f) = $(1,1)$ which corresponded to the SM prediction lies within 1ÏČ confidence level of the observed best fit value, showing the consistency of the observed boson's coupling to fermions and vector bosons with the SM expectation. Further compatibility tests were performed on other κ values and yielded results consistent with the SM prediction, they can be found in the appendix.

The diphoton decay mode indicates a non-unity value for the spin of the observed boson, spiking the 2 main alternative theories of the boson acquiring a spin of 0^+ or 0^-. An identical test regarding the difference in χ^2 tests of both parity likelihoods was

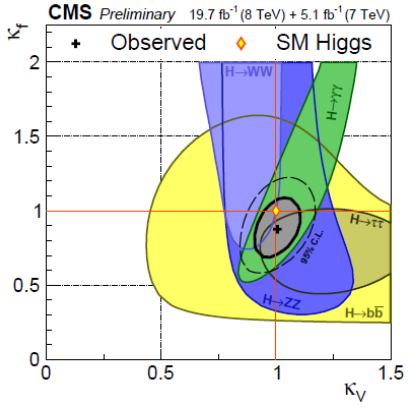

Figure 4.10.: 2D likelihood scan was performed on κ_f and κ_γ simultaneously by the CMS collaboration.

performed[42] using a test statistic formula similar to that of (eq. 2.19), but replacing the ratio in the parenthesis to that of $\frac{L_{0^-}}{L_{0^+}}$.

The results (Figure 4.11)[42] suggest a favour towards the 0^+ hypothesis as supposed to the 0^- hypothesis.

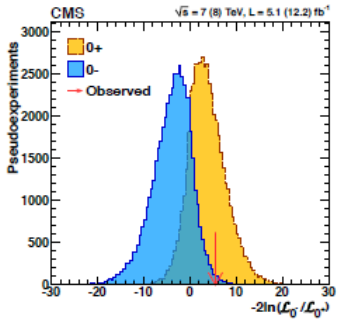

Figure 4.11.: Observed test statistic of the parity likelihood differences compared to that expected under individual parity cases.

5 Conclusion

After more than 4 decades of search and some near catches observed by the Tevatron, the SM Higgs boson was independently discovered in the summer of 2012 by the CMS and ATLAS collaborations in the LHC, with the former observing the boson at a mass of 125.3 ± 0.4 GeV/c^2 and the latter 126.0 ± 0.4 GeV/c^2.

The conclusion that the observed boson was indeed the SM Higgs was because its properties were consistent with SM predictions because its observed mass lies within limits set previously by the LEP and Tevatron. Its observed properties such as its spin parity of 0^+ and its couplings to different particles were also in agreement with SM predictions.

It should be noted that the SM Higgs boson is only one of the explanations to electroweak symmetry breaking. Various Beyond Standard Model (BSM) theories have attempted to explain the phenomena, such as the theory of there being multiple Higgs bosons[43]. New runs at the LHC has already been conducted to further investigate this, with data obtained such as that obtained in appendix looking promising.

While the travel has halted, the journey has not. With the search of the Higgs boson nearing an end, it is perhaps time for the LHC to focus on other projects such as exploring the nature of dark matter. Hopefully, significant discoveries such as this will continue to happen and humans can finally understand 10% of the Universe.

A Appendix

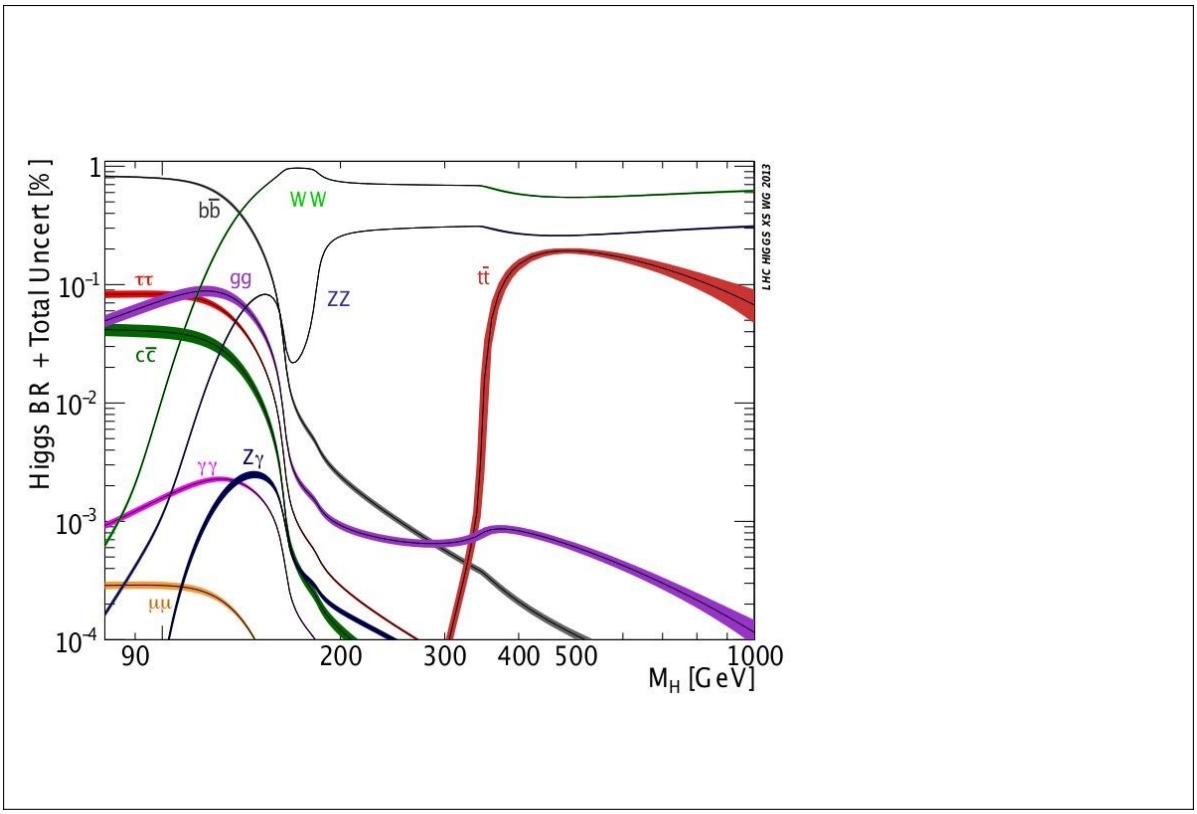

Figure A.1.: Branching ratios of different higgs decay modes

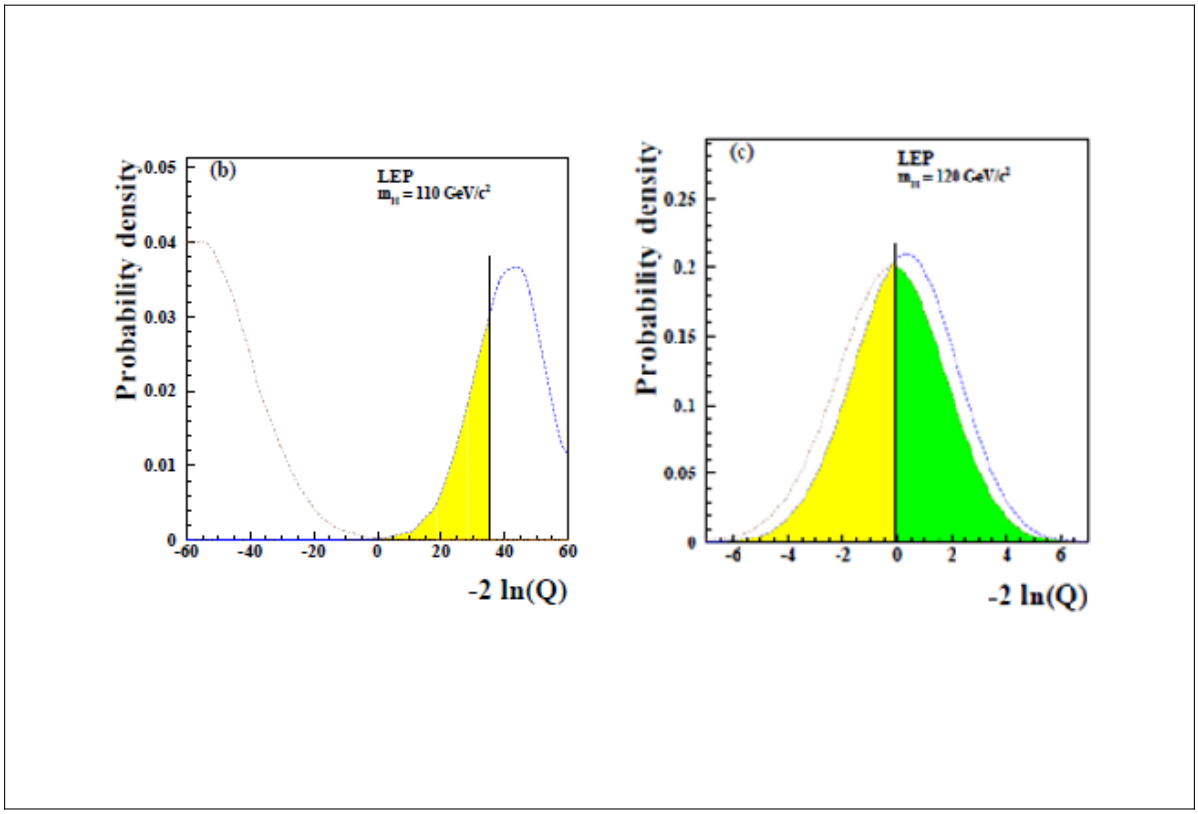

Figure A.2.: Test statistic spread for MH=110 GeV/c^2 (left) and $M_H = 120$ GeV/c^2(right)

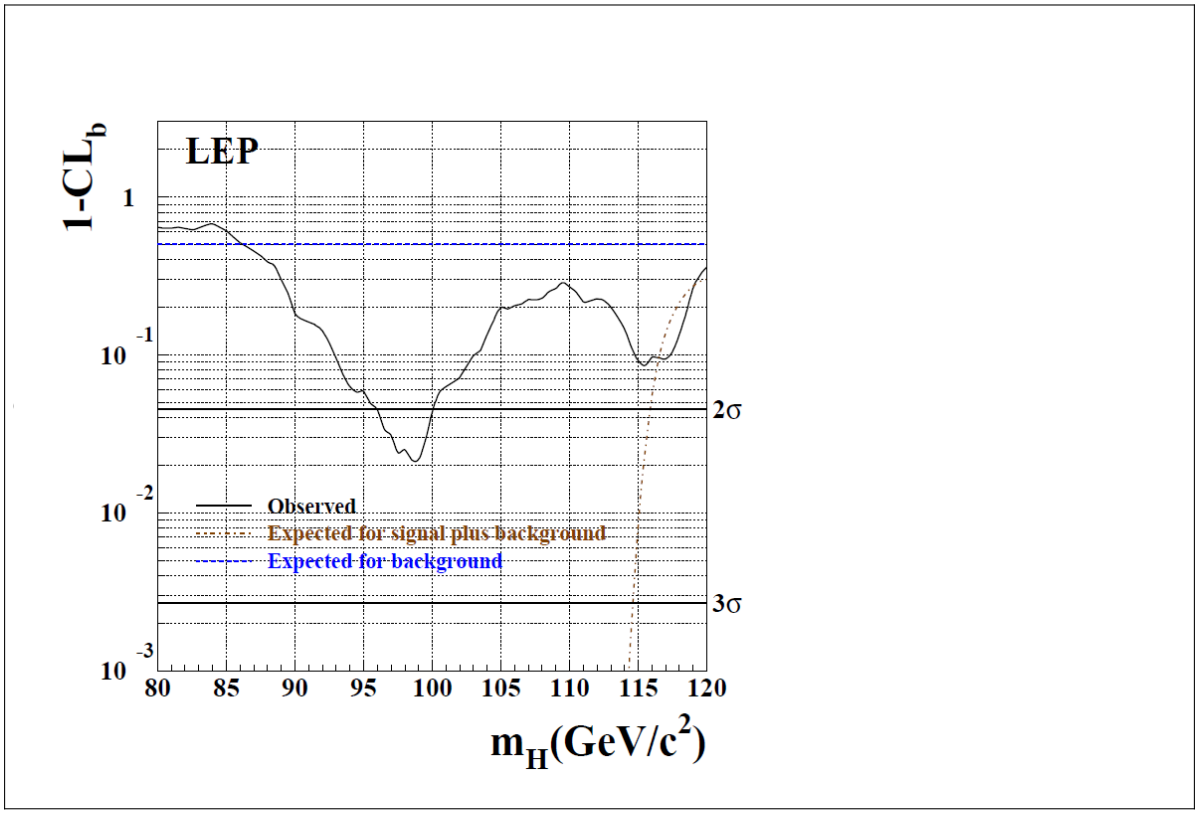

Figure A.3.: Observed $1 - CL_b$ values and their corresponding significances in the LEP

m_H (GeV/c^2)	LLR_{obs}	LLR_{s+b}	$\mathrm{LLR}_b^{-2\sigma}$	$\mathrm{LLR}_b^{-1\sigma}$	LLR_b	$\mathrm{LLR}_b^{+1\sigma}$	$\mathrm{LLR}_b^{+2\sigma}$
90	17.02	−7.24	17.31	12.08	6.84	1.61	−3.62
95	13.07	−5.96	15.21	10.44	5.68	0.91	−3.85
100	8.39	−7.44	17.73	12.40	7.08	1.76	−3.56
105	3.62	−6.69	16.38	11.35	6.32	1.29	−3.74
110	2.53	−5.73	14.79	10.12	5.45	0.78	−3.89
115	−3.67	−4.81	13.17	8.88	4.59	0.31	−3.98
120	−8.44	−4.09	11.76	7.82	3.88	−0.06	−4.00
125	−7.72	−3.52	10.76	7.07	3.39	−0.29	−3.97
130	−3.74	−3.30	10.31	6.74	3.18	−0.39	−3.95
135	−4.81	−3.64	10.89	7.17	3.45	−0.26	−3.98
140	−5.08	−4.09	11.72	7.79	3.86	−0.07	−4.00
145	0.20	−5.07	13.35	9.02	4.69	0.36	−3.97
150	3.72	−6.68	15.87	10.95	6.04	1.12	−3.79
155	8.44	−8.80	18.72	13.18	7.65	2.12	−3.41
160	13.45	−15.25	26.04	19.08	12.12	5.15	−1.81
165	17.33	−17.81	28.76	21.31	13.87	6.42	−1.03
170	10.93	−12.26	22.87	16.50	10.13	3.77	−2.60
175	7.33	−8.77	18.50	13.02	7.53	2.04	−3.45
180	4.86	−6.17	14.87	10.18	5.50	0.81	−3.88
185	2.14	−3.92	11.23	7.42	3.62	−0.19	−3.99
190	−0.99	−2.61	8.73	5.60	2.46	−0.68	−3.81
195	−2.83	−1.98	7.34	4.60	1.87	−0.87	−3.60
200	−2.50	−1.53	6.29	3.88	1.46	−0.96	−3.37

Figure A.4.: LLR observed and expected values for Tevatron

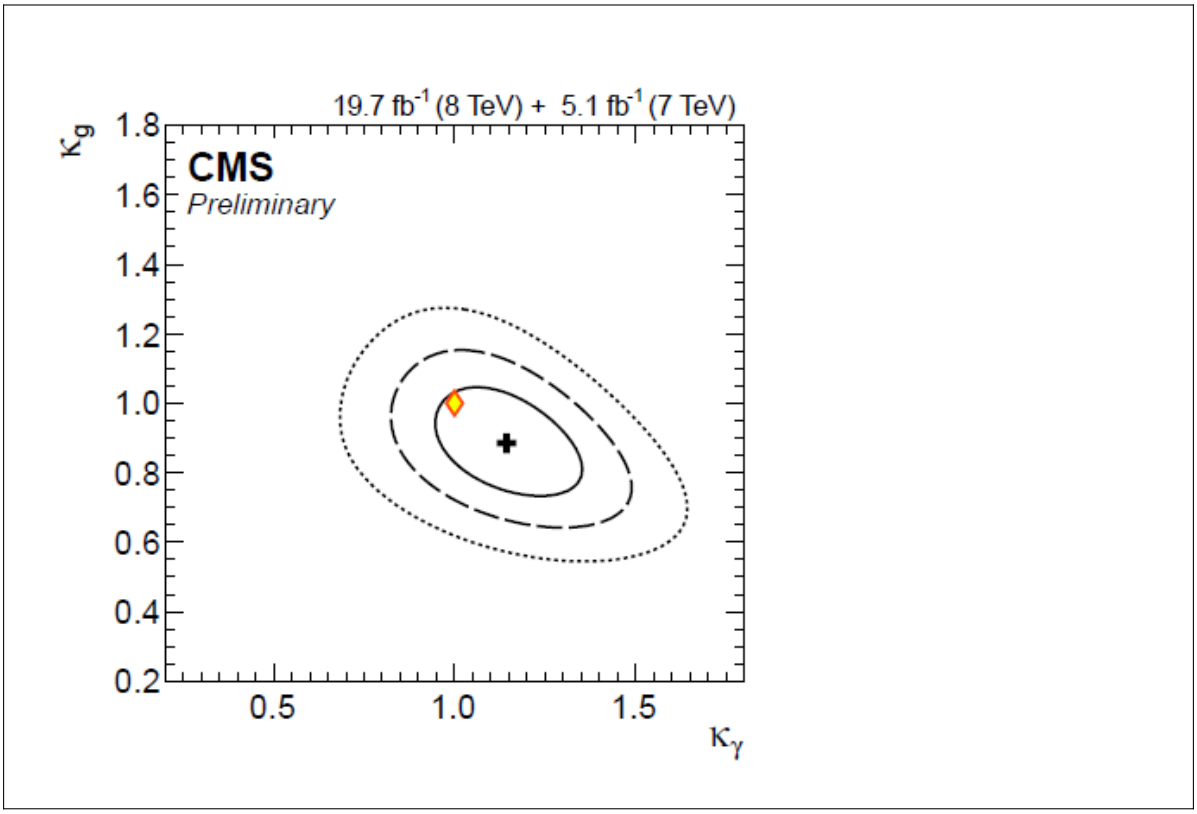

Figure A.5.: Likelihood scan between κ_γ and κ_g

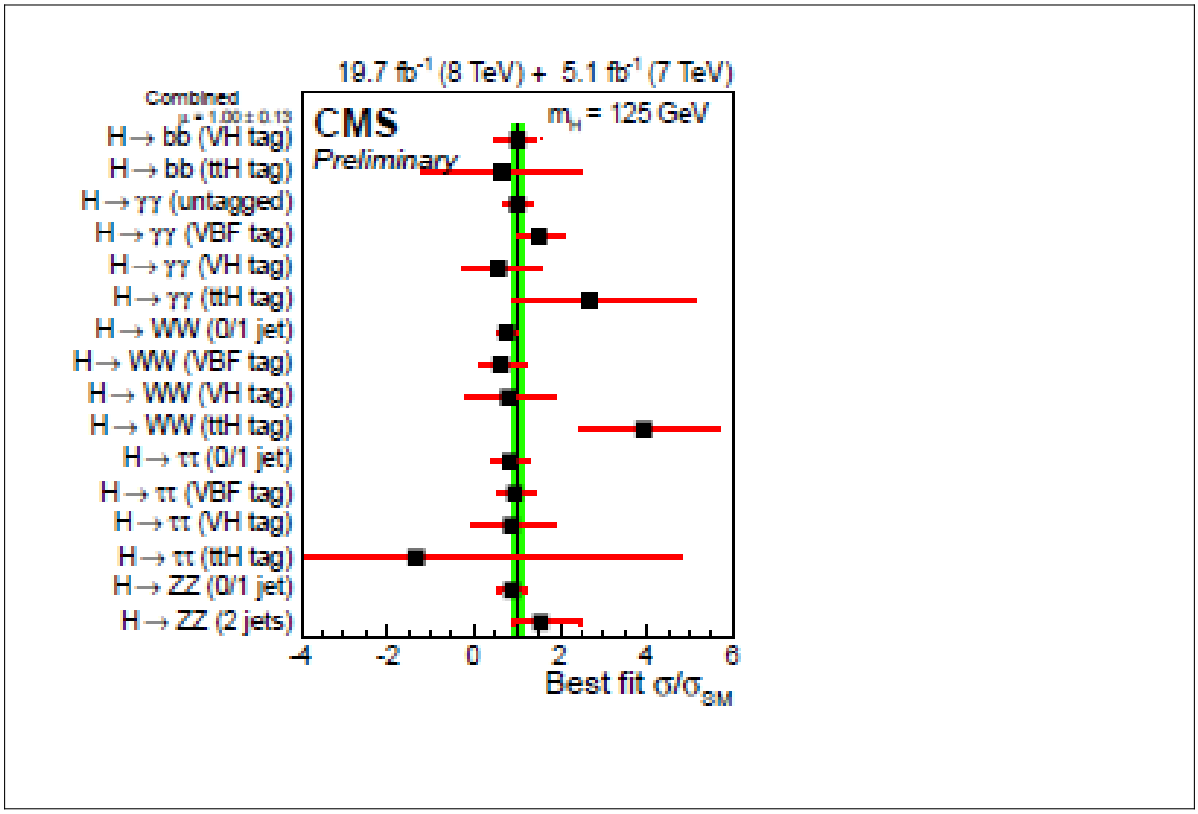

Figure A.6.: Further μ values computed at CMS with production taggings

Bibliography

List of figures

References:

1. Englert, F.; Brout, R. (1964). "*Broken Symmetry and the Mass of Gauge Vector Mesons*". Physical Review Letters. **13** (9): 321–23.
2. Higgs, P. (1964). *"Broken Symmetries and the Masses of Gauge Bosons". Physical Review Letters*. **13** (16): 508–509
3. Guralnik, G.; Hagen, C. R.; Kibble, T. W. B. (1964). "Global Conservation Laws and Massless Particles". *Physical Review Letters*. **13** (20): 585–587
4. P. W. Anderson (1962). "Plasmons, Gauge Invariance, and Mass". *Physical Review*. **130** (1): 439–442
5. Dittmaier, S. and Schumacher, M. (2013). "*The Higgs boson in the Standard Model—From LEP to LHC: Expectations, Searches, and Discovery of a Candidate"*
6. Gunion, John (2000). *The Higgs Hunter's Guide* (illustrated, reprint ed.). Westview Press. pp. 1–3
7. Lee, B., Quigg, C. and Thacker, H. (1977). Weak interactions at very high energies: The role of the Higgs-boson mass. *Physical Review D*, 16(5).
8. Weinberg, S. (1976). Mass of the Higgs Boson. *Physical Review Letters*, 36(6).
9. Ellis, J., Gaillard, M. and Nanopoulos, D. (1976). A phenomenological profile of the Higgs boson. *Nuclear Physics B*, 106.
10. Hamilton, K., Nason, P., Re, E. and Zanderighi, G. (2013). NNLOPS simulation of Higgs boson production. *Journal of High Energy Physics*, 2013(10).
11. Twiki.cern.ch. (2018). *CERNYellowReportPageBR < LHCPhysics < TWiki*. [online] Available at: https://twiki.cern.ch/twiki/bin/view/LHCPhysics/CERNYellowReportPageBR
12. Lamb, E. (2018). *5 Sigma What's That?*. [online] Scientific American Blog Network. Available at: https://blogs.scientificamerican.com/observations/five-sigmawhats-that/
13. Home.cern. (2018). *The Large Electron-Positron Collider | CERN*. [online] Available at: https://home.cern/about/accelerators/large-electron-positron-collider
14. Search for the Standard Model Higgs boson at LEP. (2003). *Physics Letters B*, 565
15. Fnal.gov. (2018). *Fermilab | Tevatron | Accelerator*. [online] Available at: http://www.fnal.gov/pub/tevatron/tevatron-accelerator.html [Accessed 16 Jan. 2018].
16. Fnal.gov. (2018). *Fermilab | Tevatron | Interactive Timeline*. [online] Available at: http://www.fnal.gov/pub/tevatron/milestones/interactive-timeline.html
17. Tuchming, B. (2013). Tevatron Higgs results. *EPJ Web of Conferences*, 60
18. Davies, G. (2013). Higgs boson searches at the Tevatron. *Frontiers of Physics*, 8(3)
19. T. Sj¨ostrand, S. Mrenna, and P. Skands, J. High EnergyPhys. 05 (2006) 026. We use pythia version 6.216 to generate the Higgs boson signals
20. M. Mangano, M. Moretti, F. Piccinini, R. Pittau, and A. Polosa, J. High Energy Phys. 07 (2003) 001.
21. E. Boos, V. Bunichev, M. Dubinin, L. Dudko, V. Ilyin, A. Kryukov, V. Edneral, V. Savrin, A. Semenov, and A. Sherstnev, Nucl. Instrum. Methods Phys. Res., Sect A 534, 250 (2004); E. E. Boos, V. E. Bunichev L. V. Dudko, V. I. Savrin, and A. V. Sherstnev, Phys. Atom. Nucl. 69, 1317 (2006).
22. H. L. Lai et al., Eur. Phys. J. C 12, 375 (2000); J. Pumplin et al., J. High Energy Phys. 07 (2002) 012.

23. A. D. Martin, W. J. Stirling, R. S. Thorne, and G. Watt, Eur. Phys. J. C 63, 189 (2009).
24. Home.cern. (2018). *CMS* | *CERN*. [online] Available at: https://home.cern/about/experiments/cms
25. Cms.web.cern.ch. (2018). *Silicon Pixels* | *CMS Experiment*. [online] Available at: http://cms.web.cern.ch/news/silicon-pixels
26. Cms.web.cern.ch. (2018). *Electromagnetic Calorimeter* | *CMS Experiment*. [online] Available at: http://cms.web.cern.ch/news/electromagnetic-calorimeter
27. Cms.web.cern.ch. (2018). *Hadron Calorimeter* | *CMS Experiment*. [online] Available at: http://cms.web.cern.ch/news/hadron-calorimeter
28. Cms.web.cern.ch. (2018). *Muon Detectors* | *CMS Experiment*. [online] Available at: http://cms.web.cern.ch/news/muon-detectors
29. ATLAS Experiment at CERN. (2018). *Calorimeter* | *ATLAS Experiment at CERN*. [online] Available at: https://atlas.cern/discover/detector/calorimeter
30. Home.cern. (2018). *ATLAS* | *CERN*. [online] Available at: https://home.cern/about/experiments/atlas
31. Alioli, S., Nason, P., Oleari, C. and Re, E. (2009). NLO Higgs boson production via gluon fusion matched with shower in POWHEG. *Journal of High Energy Physics*, 2009(04),
32. Nason, P. and Oleari, C. (2010). NLO Higgs boson production via vector-boson fusion matched with shower in POWHEG. *Journal of High Energy Physics*, 2010(2).
33. Bozzi, G., Catani, S., de Florian, D. and Grazzini, M. (2003). The qT spectrum of the Higgs boson at the LHC in QCD perturbation theory.
34. CMS Collaboration, (2013). *Observation of a new boson at a mass of 125 GeV with the CMS at the LHC*
35. CMS Collaboration (2014). Precise determination of the mass of the Higgs boson and studies of the compatibility of its couplings with the Standard Model
36. Nucl. Instrum. Meth (2005) Studies of boosted decision trees for MiniBooNE particle identification",
37. CMS Collaboration (2009), "Particle–Flow Event Reconstruction in CMS and Performance for Jets, Taus, and Emiss T ", CMS Physics Analysis Summary CMS-PAS-PFT-09-001
38. CMS Collaboration (2010), "Commissioning of the Particle-flow Event Reconstruction with the first LHC collisions recorded in the CMS detector"
39. A. Djouadi, J. Kalinowski, and M. Spira (1998), *HDECAY: A program for Higgs boson decays in the standard model and its supersymmetric extension*,
40. A. Bredenstein, A. Denner, S. Dittmaier, and M. M. Weber, *Precise predictions for the Higgs-boson decay $H \to WW/ZZ \to 4$ leptons*, Phys. Rev. **D74** (2006)
41. The Atlas Collaboration (2012). Observation of a New Particle in the Search for the Standard Model Higgs Boson with the ATLAS Detector at the LHC
42. The CMS Collaboration (2013) Study of the mass and spin-parity of the Higgs boson candidate via its decay to Z boson pairs
43. Igor Ivanov (2015). Towards systematic exploration of multi-Higgs-doublet methods.

44. de Boer, W. (2018). *The Discovery of the Higgs Boson with the CMS Detector and its Implications for Supersymmetry and Cosmology*. [online] Inspirehep.net. Available at: http://inspirehep.net/record/1252561/plots [Accessed 16 Jan. 2018].
45. Statistics How To. (2018). *68 95 99.7 Rule in Statistics*. [online] Available at: http://www.statisticshowto.com/68-95-99-7-rule/ [Accessed 16 Jan. 2018].